Tellus (1999), 51A, 249–262
Printed in UK – all rights reserved

TELLUS
ISSN 0280–6495

A shallow, short-lived meso-β cyclone over the Gulf of Antalya, eastern Mediterranean

By P. ALPERT*, M. TSIDULKO and D. ITZIGSOHN, [1]*Department of Geophysics and Planetary Sciences, Tel-Aviv University, Israel 69978*

(Manuscript received 7 January 1998; in final form 12 October 1998)

ABSTRACT

The physical mechanisms of a shallow short-lived meso-β scale cyclone over the Gulf of Antalya, eastern Mediterranean, are studied, with the PSU/NCAR MM4 and MM5 meso-scale models. Although the thin stratus clouds within this cyclone as observed from satellites are not resolved even by the 3 km nesting, the dynamical evolution and the 3-D structure are well captured. The small cyclone or eddy develops before sunrise following convergence of the strong katabatic winds from the nearby steep Anatolya mountains slopes with 2 km peaks. The eddy's lifetime is of the order of 5–7 h and it quickly dissipates before noon. Based on the simulated vertical winds, vorticity, humidity as well as the IR top cloud temperatures, the depth of the eddy is estimated to be 500–800 m. It is shown that the divergence term in the vorticity equation is dominant during the eddy's generation. Lagrangian analysis for the trajectories of several air-masses that were identified as crucial for the eddy's development, reveals a sharp increase both in the PV (by 7–8 units), and in the specific humidity, 3.5 to 7 g/kg, as the air-parcels descend from about 840 to 980 hPa. This air-parcel analysis also shows that the diabatic contribution is quite important. Factor separation experiments confirm that pure topography is the major factor and the synergistic effect of sea-fluxes and topography contributes about 20% of the total vorticity. The Antalya cyclone is common during July to September morning hours and its frequency of occurrence was estimated from satellite pictures to be about 20%.

1. Introduction

The origin and generation mechanisms of meso-scale cyclones or eddies became of increased interest in recent years as satellites provide us with high-resolution pictures and the nested meso-scale modeling became more accessible to many researchers. Small scale eddies are still mostly unresolved by nearly all the operational numerical weather prediction systems even though their significance for prediction of wind, air pollution, cloudiness and sometimes severe weather cannot be overestimated. In such cases, local forecasts may go completely astray because of such eddies.

They are common in coastal areas and were therefore sometimes entitled "Coastal Whirls", Scorer and Verkaik (1989). A number of studies on such eddies along the coast of southern California were carried out, i.e., Bosart (1983), Mass and Albright (1989) and Douglas and Kessler (1991). Kessler and Duglas (1991) identify three types of low-level circulations along the California coast. The Gaviota Eddy (Douglas and Kessler,1991), a morning eddy at the west of the Santa-Barbara Channel; The Catalina Eddy (Bosart, 1983; Mass and Albright, 1989), stretching along the California coast; And the third one, the Mid-channel Eddy, a nocturnal eddy over the Santa Barbara Channel.

These eddies should be differentiated from the

* Corresponding author.

larger but still mesoscale cyclones involved with deep convection and sometimes having tropical-cyclone-like characteristics. Several such cases have recently been noted in the literature (Billing et al. 1983; Ernst and Matson, 1983; Mayengon, 1984; Rasmussen and Zick, 1987; and Blier and Ma, 1996). In contrast, the Antalya cyclone is smaller in both the horizontal and the vertical scales and seem not to be associated with any severe weather due to the strong and persistent sub-tropical subsidence as discussed later. The Antalya eddy is also different in its characteristics from the small-scale cold cyclones identified by Alpert and Neeman through an objective classification of E. Mediterranean cyclones, Alpert and Neeman (1992); these cyclones are larger and may even be detected in synoptic datasets.

Here, we wish to explore for the first time the physical mechanisms of the Antalya Cyclone. From satellite pictures it becomes clear that it is an early morning short-lived meso-beta scale cyclone or eddy over the Gulf of Antalya, eastern Mediterranean, at the Turkish coast with a horizontal scale of 40–100 km and vertical depth of only few hundred meters within the planetary boundary layer. (The "star" in the inset map of Fig. 4 denotes its geographical location.) Our forthcoming simulations suggest that these typically weak circulation systems carry maximum wind speeds of about 6–8 m s^{-1}. The multitude of Mediterranean coastal whirls on different scales from the smallest to the synoptic scale is not new. Scorer and Verkaik (1989) describe the Mediterranean Sea in ancient times, "To them (our ancestors) it was the Ocean. It was full of unpredictable winds, now visible to us in the shallow layer held under an inversion and trapped like a lake by the surrounding mountains. Each coast becomes known for its particular eddies, many of which are described in ancient classical literature." Nowadays, besides being able to view this eddies in satellite pictures *when* clouds are formed, it will be shown how two-way interactive nested meso-scale models can be useful to discover not only the temporal evolution of the 3-D structure, but also to explore the probable mechanisms of generation (Section 3 and 4). A recent powerful trajectory program, i.e., Schär and Wernli (1993), will also be employed (Section 5) to follow the air-parcels into the eddy and their thermodynamics Lagrangian characteristics that play the central role in the cyclone's evolution.

2. The Antalya cyclone

Fig. 1 shows the NOAA satellite near infra-red image over the eastern Mediterranean on 8 July 1993, 0826 LT (0526 UTC with daylight saving time). Over the Gulf of Antalya west-northwest to Cyprus (36.5°N, 30.5°E) a sharp eye may notice a small whirl about 40 km in diameter, although an unexperienced eye may mistook it to another small Mediterranean island which really does not exist. A zoom over the Gulf of Antalya, Fig. 2, reveals a beautiful meso-β scale cyclone. Figs. 2a–c show three consecutive NOAA satellite pictures at 06:52, 08:26 and 09:24 LT, respectively. The pictures are in the near IR, visible and visible of NOAA10, NOAA12 and NOAA9, respectively. The cyclone was generated before sunrise (i.e., about 0540 LT), at around 0400 LT, and quickly dissipated after sunrise with a lifetime of about 5–7 h. Fig. 2c is just before the eddy has completely dissipated. Fig. 3 presents another occasion on the 12 September, 1993, 06:07 LT with a slightly larger eddy. This is just before sunrise time (about 06:17 LT). The NOAA10 IR picture illustrates the warmer SST to the north of the eddy, i.e., the darker sea as compared to more southerly regions. A consistent search for such eddies during the month of August 1995 yielded 6 out of 28 days where suitable satellite data was available. The months of July, August and September were explored in the year 1995 and this has revealed a similar frequency of occurrence of about 20%. The temperature differences between the stratus tops and the neighboring SST in several cases were examined and found of the order of 4–6° suggesting approximate cloud tops of 600–750 m. The relative fast dissipation in the early morning hours indicates a thin cloudy layer of the order of one hundred meters. This is just about all information deduced from the satellite pictures. Next section describes the hydrostatic meso-scale modeling results.

3. Hydrostatic model simulations

3.1. Model aspects

The model employed here is the PSU/NCAR meso-scale model version 4 (MM4) and is

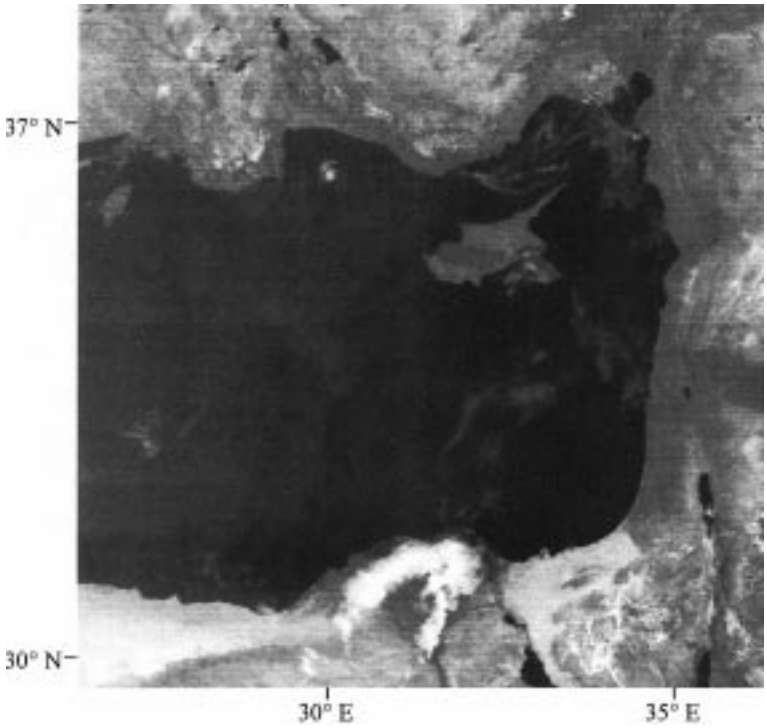

Fig. 1. NOAA12 satellite visible image over the eastern Mediterranean on 8 July 1993 0826 LT (0526 UTC). Full horizontal scale of the picture is 900 km.

described along with the parameterizations by Stein and Alpert (1991, 1993). The non-hydrostatic MM5 version as described by Grell et al. (1994), is employed in the next section. The horizontal grid-interval for the hydrostatic run was 10 km with 15 levels and a 41 × 41 grid covering a region of 400 × 400 km as shown in Fig. 4. Model topography shown is based on the US Navy 10 minutes topography from NCAR. The equivalent horizontal interval over Antalya is of about 17 km. Initial fields were from the British Met. Office and with a single radiosonde over Turkey (indicated by an "X") used for the meso-scale model initialization, Fig. 4. The lateral boundaries were also updated by the British Met. Office operational analyses provided by the Israel Meteorological Service. The introduction of the radiosonde follows the routine in MM5 as follows. The objective analysis performed in RAWINS (program to incorporate rawinsonde data) is based on the Cressman scheme, in which several succesive scans nudge a first-guess field toward the observations. Simulation started at 0000 UTC 12 Sept 1993 and run for 12 h.

3.2. *Model results*

Figs. 5a–d show the surface wind fields for 0000, 0300, 0600 and 0900 UTC respectively. At 0300 UTC or 0600 LT (Fig. 5b), few minutes before sunrise time, strong downslope winds developed over the slopes to the west of the Gulf (detailed topography is given in Fig. 4) with intensities exceeding 5 m s^{-1}. These winds are deflected in the cyclonic sense over the Gulf of Antalya. The formation of a surface vortex is complete at 0900 LT (0600 UTC), as illustrated in Fig. 5c. Location is about 30 km to the northwest compared to the observed satellite vortex in Fig. 3. The simulated temporal evolution seems quite close to that deduced from the satellite pictures observations for the July case in Fig. 2. The shift in the location may be due to the inadequate resolution in the initial fields as well as exact timing of the cyclone's

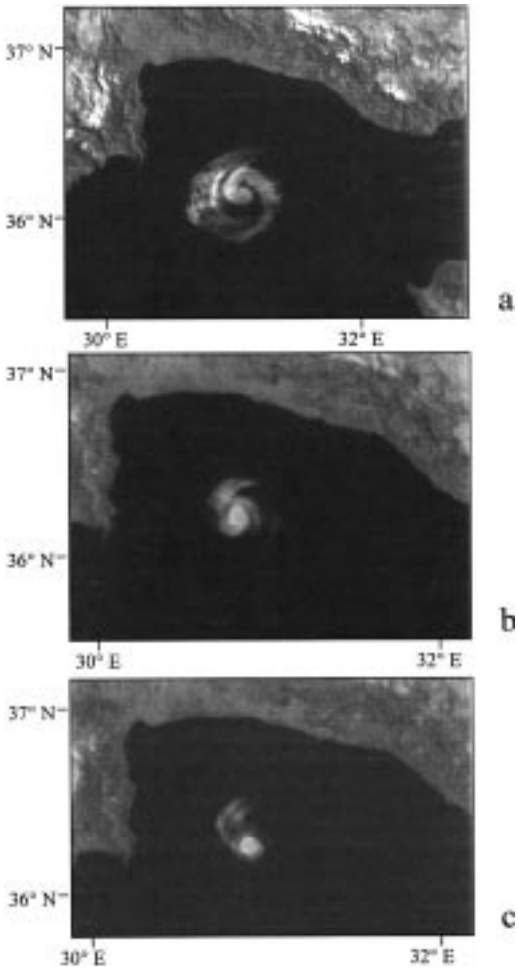

Fig. 2. Satellite images over the eastern Mediterranean on 8 July 1993 with a zoom over the Gulf of Antalya. (a) NOAA10 NIR; 0652 LT (0352 UTC), (b) NOAA12 visible; 0826 LT (0526 UTC), (c) NOAA9 visible; 0924 LT (0624 UTC). Full E–W horizontal scale of the picture is 250 km (a) and 200 km (b,c).

evolution. Actually, it was quite surprising to find that a 10 km spacing was capable at all to show any vortex generation with a typical diameter of 40–70 km. The hydrostatic model results (for winds only) were presented by Alpert et al. (1994). Next section describes nesting with a 3 km spacing using the non-hydrostatic MM5 version as well as further investigation of the simulated vorticity, humidity, vertical velocity and the airmass trajectories leading right into the cyclone's center.

4. Non-hydrostatic nested model simulations

4.1. Model aspects

The coarse and nested grids use 9 and 3 km spacings respectively. It was run in a two-way interactive mode with the same initialization as described earlier. Ten sigma levels were chosen below 1000 m with an approximate vertical spacing of 100 m with a total of 23 levels and the intervals quickly increasing with height above 1 km. The radiation effects due to clouds were parametrized, the surface land-use parameters were assumed variable and the Blackadar PBL parametrization was used. The simple radiative cooling option was chosen and the relaxation inflow/outflow boundary conditions were used. Implicit Kuo cumulus parameterization scheme was used for the coarse (9 km) domain and explicit moisture scheme without any cumulus parameterization was used for the nested (3 km) domain. Further details on the schemes and various parametrizations can be found in Grell et al. (1994).

Figs. 6a,b show each two panels; the top for the 9 km spacing and the bottom for the nested grid with 3 km; Figs. 6a,b correspond to surface wind fields at 0200 and 0600 UTC, respectively. The surface pressure drop at the cyclone's center is only of about 1.5 hPa, i.e., central pressure of about 1009 hPa (not shown). Some changes in topography, Fig. 6a, can be noticed as compared to Fig. 4, due to the slightly different grids.

4.2. Model results

As described in Section 3 for the hydrostatic run, here as well the downslope winds strengthen with time and the vortex is clearly noticed, particularly in the nested run, Figs. 6a,b. The peak is reached at 0600 UTC and afterwards the eddy quickly dissipates as also observed from the satellite pictures in Figs. 2a-c. The maximum vorticity at the center of the nested eddy reaches $159 \times 10^{-5}\ s^{-1}$ as compared to $77 \times 10^{-5}\ s^{-1}$ in the coarse grid and $83 \times 10^{-5}\ s^{-1}$ in the aforementioned hydrostatic run, Fig. 7. The maximum wind speed within a radius of about 30 km from the cyclone center is of about 6 m s^{-1} slightly increasing in the nested run to about 7 m s^{-1}.

The vertical west-to-east cross-section of the

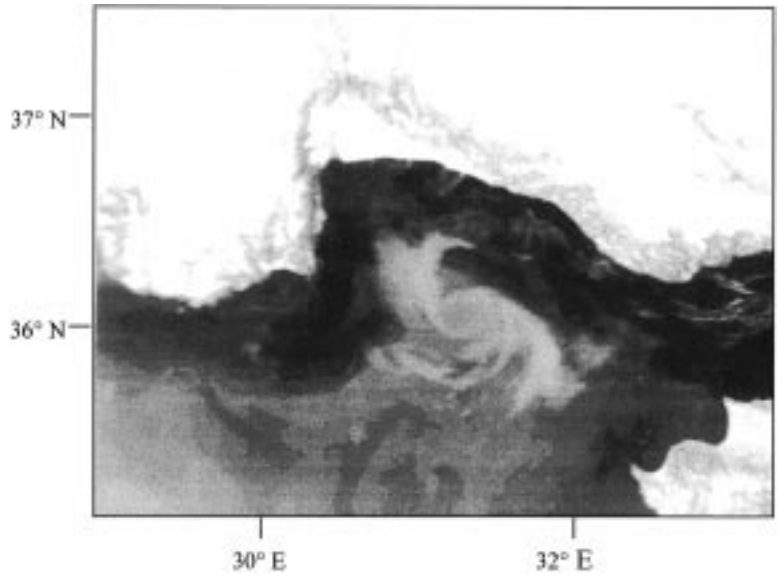

Fig. 3. NOAA10 IR image over the Gulf of Antalya on 0607 LT (0307 UTC) 12 September 1993. Full horizontal scale of the picture is 490 km.

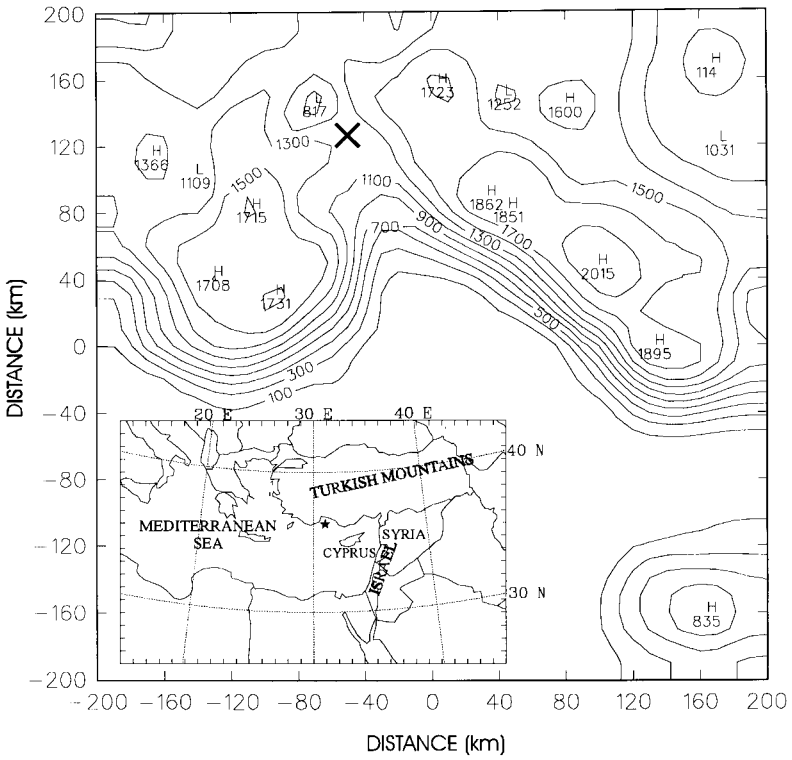

Fig. 4. Model topography for the MM4 simulation over the Gulf of Antalya with a 400 × 400 km domain. The axes' numbers indicate distance (km) from the grid center. The "X" denotes location of the single radiosonde over the model domain No. 17240. The inset map at the bottom left shows the general region and the Antalya gulf is indicated by a "star".

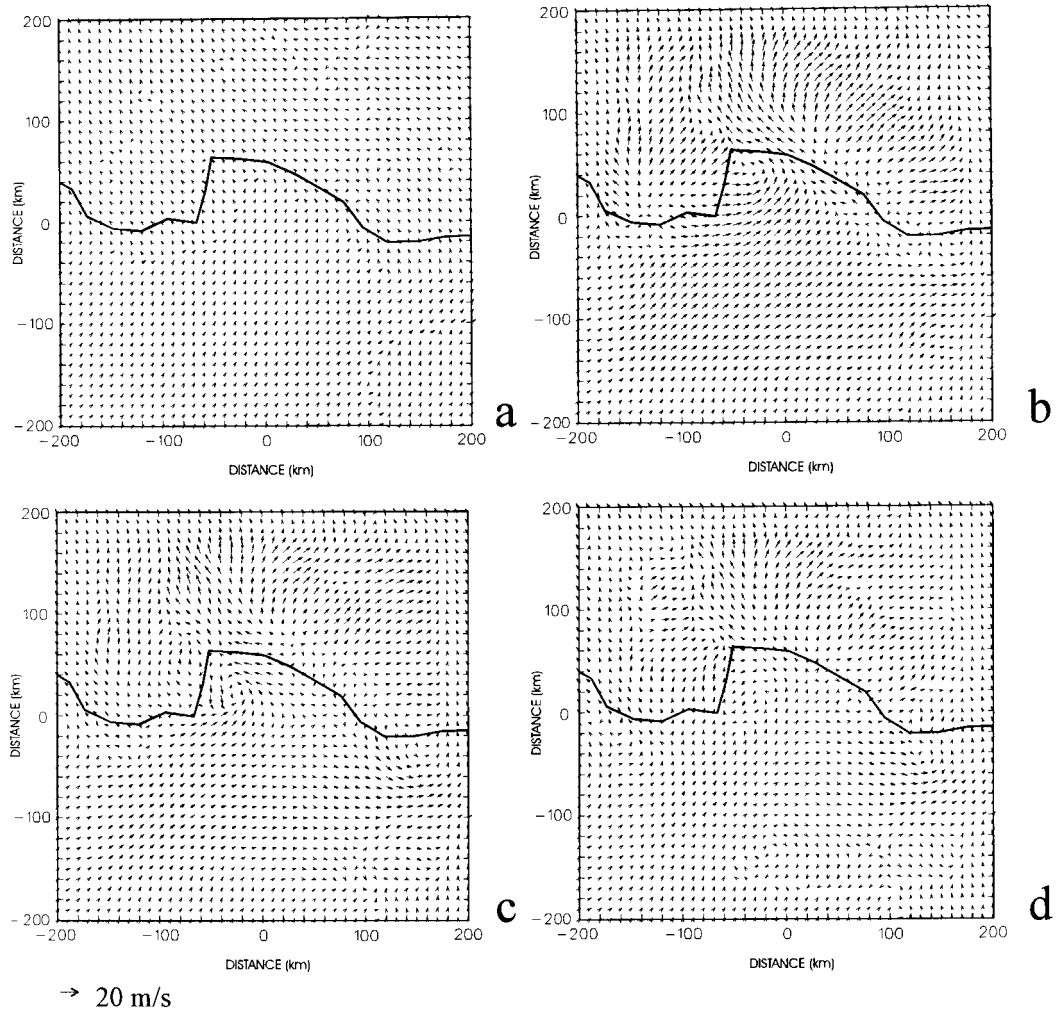

Fig. 5. Surface winds as predicted by the MM4 model simulation for: (a) 0000 UTC, (b) 0300 UTC, (c) 0600 UTC, (d) 0900 UTC. Simulation started on 0000 UTC 12 September 1993. Wind speed scale of 20 m s^{-1} is indicated at the bottom left.

horizontal vorticity field along the center of the nested vortex, Fig. 8, illustrates how shallow is the eddy attaining maximum vorticity at the surface and decreasing quickly with height by about one order of magnitude to only $10 \times 10^{-5}\,s^{-1}$ at the altitude of about 1 km or 900 hPa. Strong negative vorticity centers are noticed over the slopes and to the foothills to the west, Figs. 7, 8. The upper-levels' negative vorticity above 850 hPa is due to the dominant sub-tropical ridge which is associated with consistent subsidence through all the summer months over the eastern Mediterranean, e.g., Alpert et al. (1990).

The model did not simulate the thin cloud layer probably due to the insufficient vertical resolution with about 100 m spacing. This spacing is probably close to or even larger than the cloudy layer thickness which is unknown. The nested model however does show the increase of the humidity up to a maximum of about 75% at 50 m altitudes, Fig. 9, and at about the right location as estimated from the satellite pictures, Figs. 1, 2. The vertical

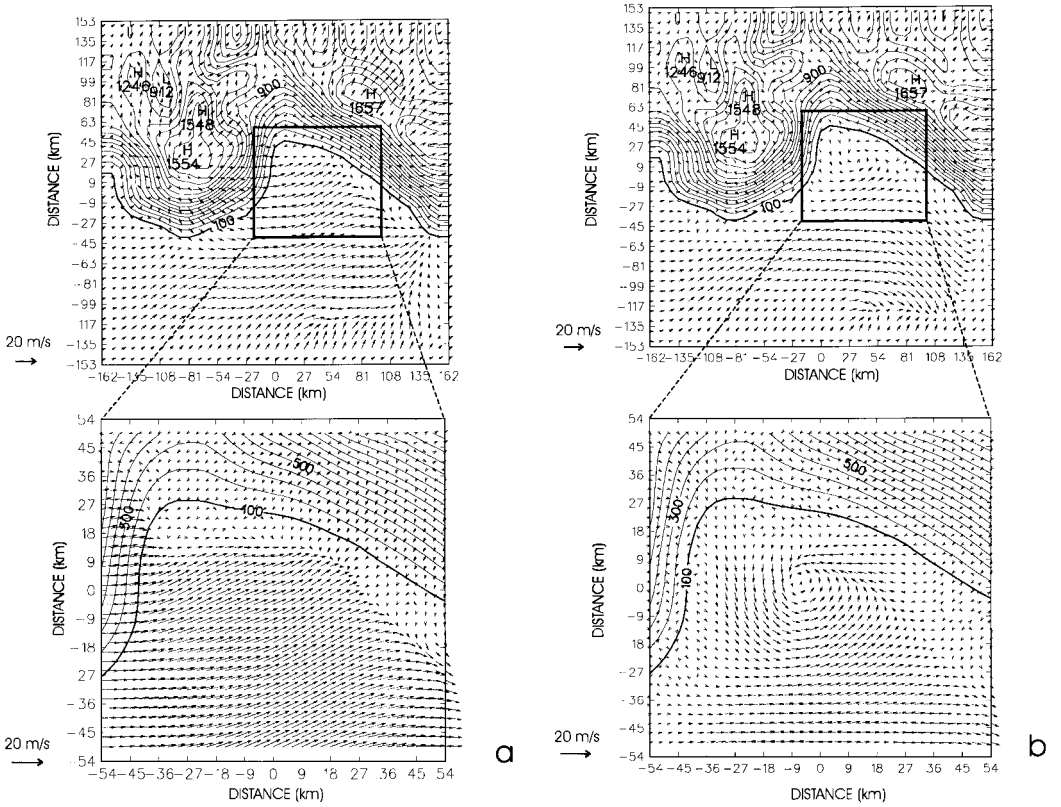

Fig. 6. MM5 simulation. Model topography and surface winds as predicted by the non-hydrostatic MM5 simulation for the coarse (upper panel) and nested (lower panel) grids. The location of the nested grid is indicated by the squares in the upper panels. Corresponding output times are, (a) 0200 UTC and (b) 0600 UTC. The simulation started at 0000 UTC 12 September 1993. Topography interval is 100 m. Wind speed scale of 20 m s^{-1} is indicated at the bottom left.

p-velocity, i.e., ω, wind field over the model cross-section, Fig. 10, illustrates the significant subsidence ($\omega > 0$) above the boundary layer and the shallow 1 km layer within the Gulf of Antalya with the upward motion at 0300 UTC (0600 LT) with maximum exceeding 1 m s^{-1} (-10 Pa s^{-1} $\sim +1$m s^{-1}). The layer of strong katabatic flow over the western slope is also noticed with the depth of a few 100s meters and fits well both theoretical predictions for the depth of the katabatic flow and some observations elsewhere, e.g., Atkinson (1981).

5. Discussion

5.1. *Vorticity generation*

The time evolution of the various terms in the vorticity equation is shown in Fig. 11. The budget was calculated for a grid-point close to the eddy's center, in the hydrostatic run, at the altitude of about 40 m. Unsurprisingly the vertical stretching term is the dominant generator of vorticity. The tendency and horizontal advection terms are both small. The vertical advection and the tilting terms were found significantly smaller than the other terms and are not shown here. The large residual reflects primarily the frictional contribution. The solenoidal term is also very small since the sigma surfaces over sea are quite close to isobaric surfaces where the solenoidal term vanishes.

Doyle and Warner (1993) similarly investigated the various vorticity terms for 5 polar lows and it is interesting to point at least two quite distinctive patterns. First, for the polar lows the contributions are significant up to about 500–600 hPa (4–5 km), whereas for the Antalya cyclone the vorticity drops

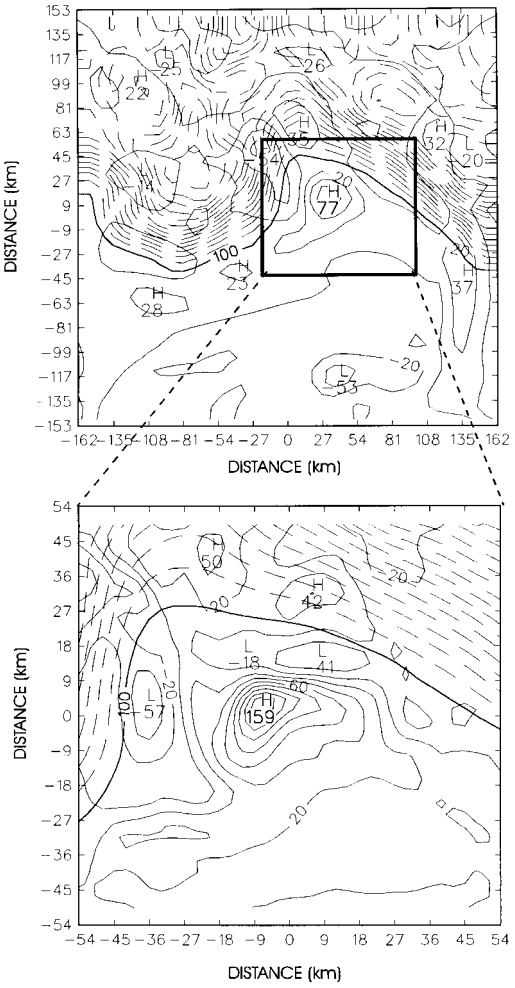

Fig. 7. MM5 simulation. Model relative vorticity ($10^{-5}\,s^{-1}$ units) in the coarse (upper panel) and in the nested (lower panel) domains at 0600 UTC. Contour interval for vorticity is 20 units. Topography is indicated by dashed lines with an interval of 100 m.

sharply above the altitude of about 1 km. Second, in the polar lows several vorticity terms are comparable to the vertical stretching term including the horizontal and vertical advection terms, the vorticity tendency and even the tilting terms while in the Antalya case the single dominant term seems to be the vertical stretching which maximizes right near the surface (not shown). Interesting to note is that for both the polar low and the Antalya Cyclone the leading term up to about 900 hPa is the same, i.e., the vertical stretching.

5.2. *Effect of the earth rotation and interactive nesting*

If indeed the vertical stretching term or the divergence term dominates the vorticity equation then,

$$\frac{\partial \xi}{\partial t} \doteq -(f+\xi)\nabla \cdot \boldsymbol{V},$$

where ξ is the relative vorticity, f the earth vorticity and $\boldsymbol{V}$, the horizontal wind vector. Hence, the inclusion of the Coriolis contribution should yield a vorticity ξ, which is larger by about the fraction of the major generation divergence terms, i.e.,

$$(f+\xi)/\xi = \left(1+\frac{f}{\xi}\right).$$

For the latitude of Antalya, i.e., 36°N, and $\xi = 46\times10^{-5}\,s^{-1}$, (the peak vorticity for $f=0$, Fig. 12) this means a 19% increase due to the Coriolis contribution. Indeed, this value is surprisingly close to the vorticity increase of 21% as simulated at 6 h, Fig. 12, for the no nesting case, i.e.,

$$\frac{\xi(f\neq 0)}{\xi(f=0)} = \frac{56}{46} = 1.21.$$

In other words, the earth vorticity has an intensifying contribution to the Antalya cyclone of about 20% and this fits very well the theoretical prediction when assuming that the divergence term prescribes the vorticity development.

It is interesting to note that the two-way interactive nesting employed here has a positive effect on the deepening of the coarser grid cyclone at around time of maximum development, i.e., 6 to 9 h, along with opposite (negative) feedbacks both earlier and later, compare the two curves with $f\neq 0$ in Fig. 12. Hence, the fine mesh seems to convey a twofold message to the coarser grid. First, the real lifetime of the cyclone is shorter and second, its peak intensity is higher. The two messages improve the coarser grid result using higher resolution information that cannot be resolved by the coarser grid alone.

5.3. *Airmass trajectories*

Figs. 13a,b show trajectories of air parcels objectively identified using the method developed by Schär and Wernli (1993). The method allows

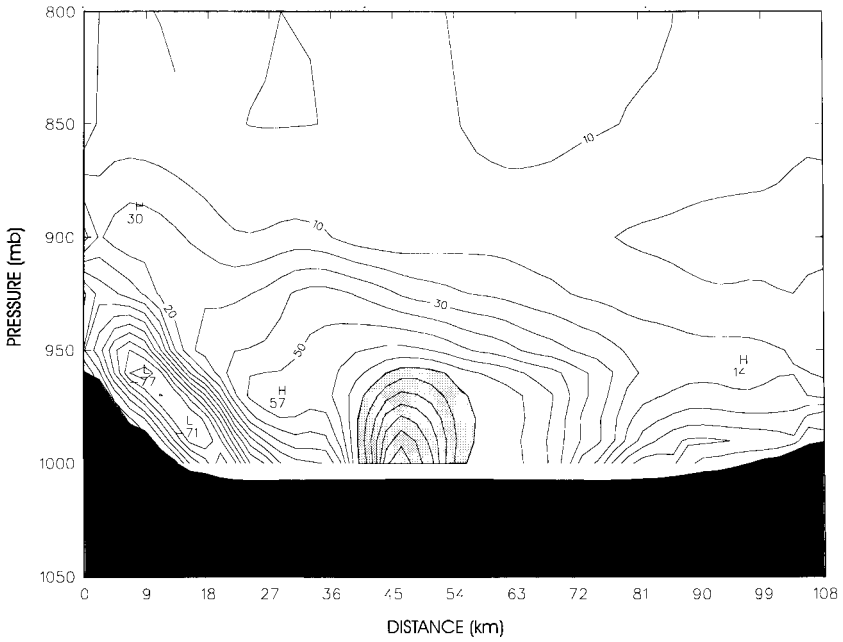

Fig. 8. MM5 simulation. Vorticity east-west cross-section through the vortex at 0600 UTC in the nested domain. Contour interval is 10 units. Shading is for values exceeding $80 \times 10^{-5}\ s^{-1}$.

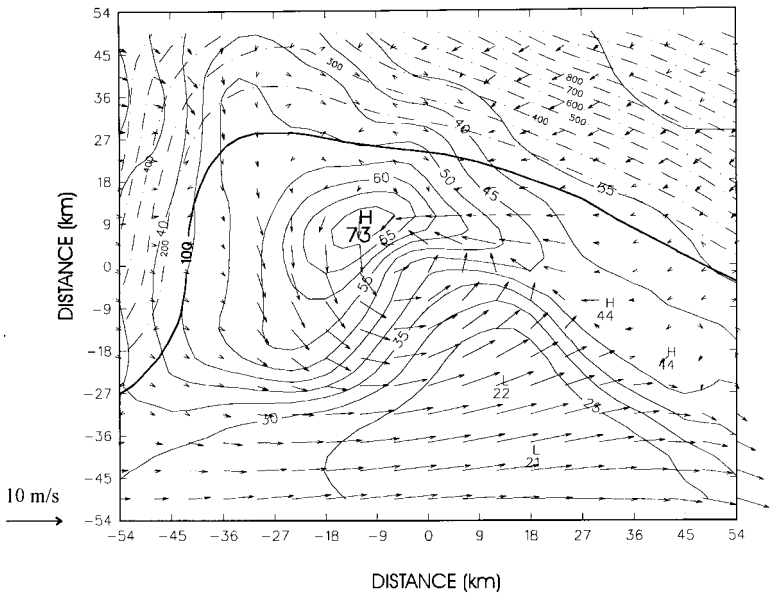

Fig. 9. MM5 simulation. Nested domain winds and relative humidities at 0600 UTC at the altitude of about 50 m above mean sea level. Relative humidity contour interval is 5%. Topography is indicated by dashed lines with 100 m interval.

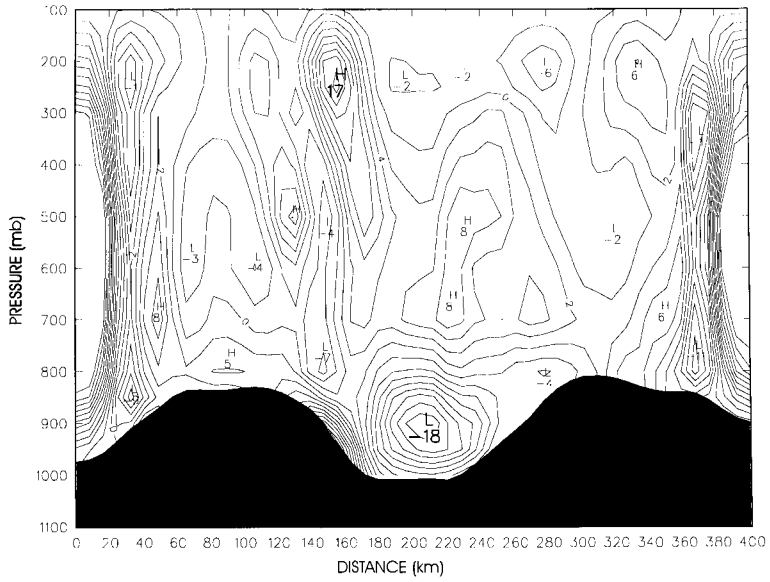

Fig. 10. MM4 simulation. East-west cross section of ω(Pa/s) at 0300 UTC with a contour interval of 2 Pa s^{-1} (+2 Pa s^{-1} ~ −0.2 m s^{-1}). Lateral boundaries disturbances can be noticed.

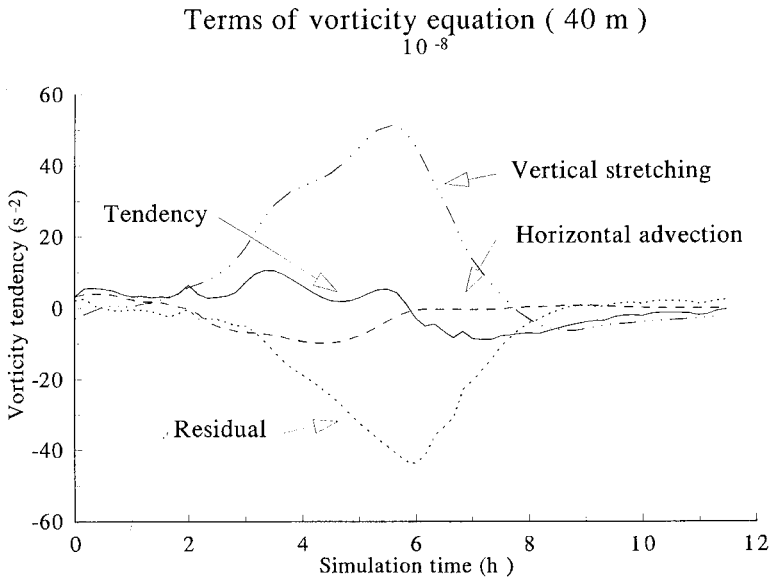

Fig. 11. Time evolution of the primary terms of the vorticity equation at one point in the vortex (close to the center at 40 m above MSL) during the 12 h simulation. Units are in 10^{-8} s^{-2}.

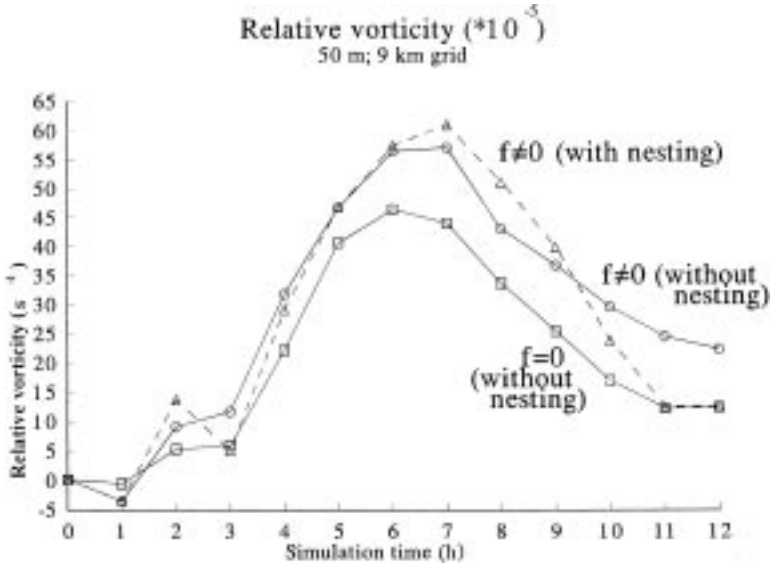

Fig. 12. Time evolution of the relative vorticity at one point near the vortex center in the MM5 simulations with (△) and without nesting (○) and with no-nesting when *f*, the Coriolis parameter equals zero (□). Vorticity units are $10^{-5}\,s^{-1}$.

the calculation of all possible trajectories starting (or ending) inside some fixed region, and then to choose only those that satisfy the criterion we wish to apply. Fig. 13 presents all the trajectories starting at grid points of the model domain between 1000 and 700 hPa at 00 GMT *and* descending a layer thicker than some selected value, within 6 h of the simulation. Hence, Figs. 13a,b show the trajectories that have descended more than 50 and 115 hPa, respectively, and most probably identify those simulated air-streams that play the central role in this case of shallow cyclogenesis. The north-eastward flow of these air-masses coincides with the direction of the synoptic scale motion. The air-masses descend along the left (western) slope of the Antalya gulf from about 1–1.5 km and interact with air-masses originating from the right slope thus increasing the convergence and leading to the cyclone's formation.

Fig. 14 focuses on the time evolution of only 14 parcels (shown in Fig. 13b) that have dropped down from the top of the mountains more than 115 hPa. The 8 K drop in the potential temperature, θ, goes along with significant increases of both the potential vorticity, PV, and the specific humidity. Clearly, both θ and PV are not conserved here and diabatic processes play their role. The air-parcels descending from 880 to 980 hPa experience a sharp increase in their specific humidity (3.5 to 6.5 g/kg), a 4 K decrease in their potential temperature and about 7 units (i.e., 2.5 to 9) PV increase.

This dramatic change in the air-parcels PV within only 6 h of simulation can be mostly explained by the vorticity increase. For instance, the vorticity increase between the origin and the final points at +6 h of the simulation (Fig. 8; vorticity cross-section) is about one order of magnitude, i.e., from 10 to 100 ($10^{-5}\,s^{-1}$ units). Hence, the relative vorticity variation is large enough to account for the total potential vorticity increase while the stability changes along the trajectories are relatively small. Of-course, the vorticity cross-section in Fig. 8 is a picture at a specific time not like the Lagrangian description here in Fig. 14, but the vorticity increases should not be much different. The dramatic PV increase must therefore be associated with diabatic effects and probably a strong frictional contribution as the air-masses penetrate into the boundary layer. The potential temperature cooling of the air-parcels could be due to the more effective radiational cooling in the moist air below.

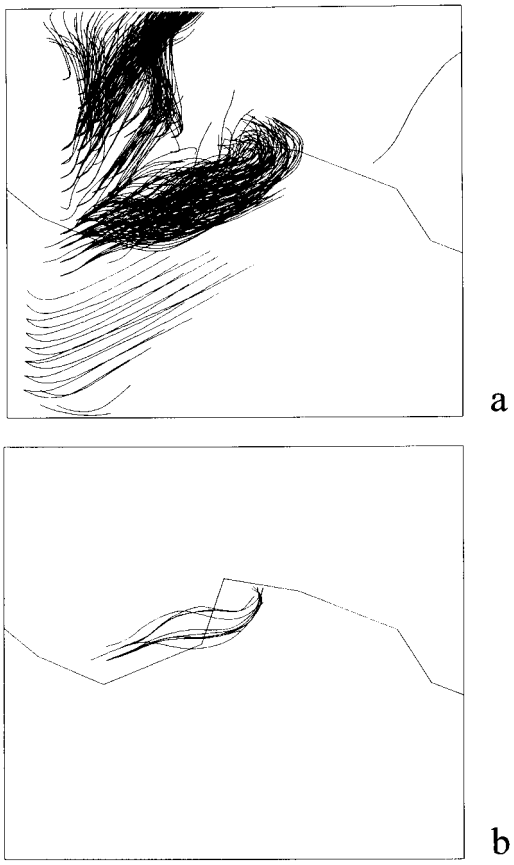

Fig. 13. Trajectories of air parcels within 700–1000 hPa descending during 0000–0600 UTC a layer thickness exceeding (a) 50 hPa, (b) 115 hPa. Trajectories of air-masses into the Gulf of Antalya play the central role in the generation of the cyclone.

6. Summary

The physical mechanisms of a shallow short-lived meso-β scale cyclone over the Gulf of Antalya, Eastern Mediterranean, as observed from zoomed satellite images, are studied. The primary tools are the PSU/NCAR meso-scale models both the hydrostatic (MM4) and the non-hydrostatic (MM5) versions. With the latter, double nesting with horizontal grid intervals of 9 and 3 km were used. The models were found capable of simulating the generation and dissipation characteristics of the eddy very well. Although the thin stratus clouds within this cyclone observed from satellites are not resolved even by the 3 km nesting, the layer of moisture increase was. In addition, the dynamical evolution and the 3-D structure are well captured particularly by the nested grid predicting a central maximum vorticity of $159 \times 10^{-5}\,s^{-1}$. The small cyclone or eddy develops before sunrise following convergence of strong katabatic winds from the nearby steep Anatolya slopes with peaks of up to 2 km. The eddy's lifetime is of the order of 5–7 h and it quickly dissipates before noon. The Antalya eddy may therefore be classified as the 3rd type nocturnal Mid-Channel eddy over the Santa-Barbara as defined by Kessler and Douglas (1991).

The divergence term in the vorticity equation is shown to be the dominant one during the eddy's generation as compared to the horizontal advection and the tendency terms. This finding is further approved by the 20% reduction in the maximum cyclone vorticity when the earth's rotation vanishes. The large residual term in the vorticity budget equation reflects probably the frictional effects.

Analysis of the crucial air-parcels trajectories that have dropped down from the top of the mountains more than 115 hPa within 6 h thus generating the meso-beta scale cyclone, was performed. The 8 K drop in the potential temperature goes along with 7 units increase of the PV, and the nearly doubling of the specific humidity from 3.5 to 6.5 g/kg. Clearly, both θ and PV are not conserved here and diabatic processes play their significant role. This PV increase can be mostly explained by the relative vorticity change which is about by one order of magnitude, i.e., from 10 to 100 ($10^{-5}\,s^{-1}$). The potential temperature cooling of the air-parcels could be due to the more effective radiational cooling in the moist air below.

The contribution of the sea-fluxes to the cyclone development was calculated using the factor separation method introduced by Stein and Alpert (1993). This method allows the isolation of the synergistic contribution. Here, the factor separation experiments confirmed that pure topography is the major factor contributing 80% of the central cyclone's vorticity while the synergistic effect of sea-fluxes and topography contributes the rest of about 20%. This value may in reality be somewhat larger since the thin stratus clouds were not captured by the model. The 20% result is clearly different from the case with larger synoptic scale Cyprus cyclones over the E. Mediterranean where the sea fluxes are the major contributor as shown by Alpert et al. (1995). Also,

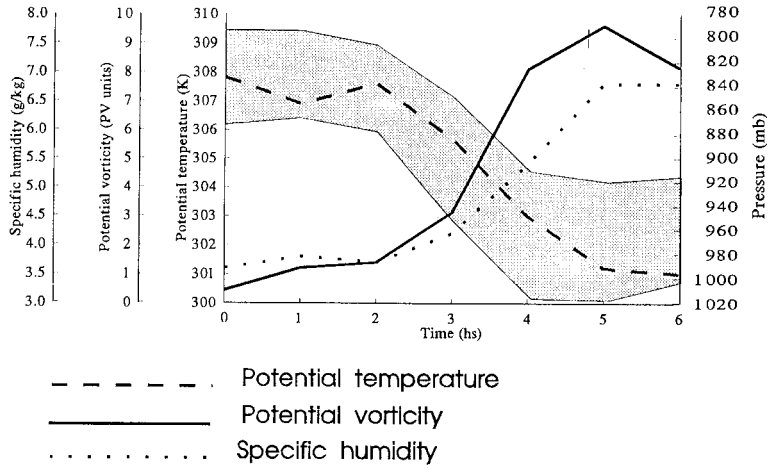

Fig. 14. Time evolution of the descending air-stream as calculated from the average of all 14 air-masses in Fig. 13c. Shaded area indicates the pressure $\pm$ standard-deviation, the other lines show specific humidity (g/kg), potential vorticity (PV units) and potential temperature (K).

no significant effect was found in the model result when the variation in the SST as inferred from the IR satellite picture were introduced into the surface boundary conditions (Fig. 3).

The contribution of the two-way interactive nesting to the development of the coarser grid cyclone was also examined. It is found that the two-way interactive nesting has a positive effect on the deepening of the coarser grid cyclone at 6 to 9 h, times of maximum deepening, along with opposite (negative) feedbacks both earlier and later. Hence, the fine mesh seems to convey a twofold message to the coarser grid. First, that the real lifetime of the cyclone is shorter and second, its peak intensity should be higher. The two messages clearly improve the coarser grid simulation through the higher resolution information that cannot be resolved by the coarser grid alone.

This Antalya cyclone is a common phenomenon with variable intensity over the Gulf of Antalya and seems to be as frequent as 20% of the summer mornings. Future studies should examine this and the reasons for such a frequency of occurrence. It might be associated with the variations in the larger scale synoptic system flows even though they are relatively small. Indeed, our preliminary experiments have shown high sensitivity to the initial wind fields.

7. Acknowledgments

The study was supported by the US-Israel Bi-national Science Foundation grant No. 92-00275. The work was partly performed while the first author (PA) held a National Research Council–NASA/GSFC Research Associateship at the Data Assimilation Office, Code 910.3, NASA/GSFC, GREENBELT, MD20771, USA. We wish to thank the National Center for Atmospheric Research (NCAR) the MESO-USER staff, and particularly Drs. Sue Chen, Wei Wang and Bill Kuo for the help in adopting the PSU/NCAR meso-scale model and its new versions at Tel-Aviv University. Thanks are due also to the Israel Met. Service for the initial and boundary conditions.

REFERENCES

Alpert, P., R. Abramsky and B. U. Neeman, 1990. The prevailing summer synoptic system in Israel — subtropical high, not Persian trough. *Israel J. Earth Sci.* **39**, 93–102.

Alpert, P. and B. U. Neeman, 1992. Cold small-scale cyclones over the eastern Mediterranean. *Tellus* **44A**, 173–179.

Alpert, P. and Y. Shay-El, 1993. The paradox of the

winter net moisture sink over the Arabian–Iraqi desert. *Annales Geophysicae* **11**, 190–194.

Alpert, P., U. Stein and M. Tsidulko, 1995. Role of sea fluxes and topography in eastern Mediterranean cyclogenesis. *The Global Atmosphere-Ocean System* **3**, 55–79.

Alpert, P., M. Tsidulko and D. Itzigsohn, 1994. A shallow short-lived meso-β scale cyclone over the gulf of Antalya. *Proceedings of the 6th Conference on Mesoscale processes*, AMS, 18–22 July, Portland, Oregon, USA, 508–509.

Atkinson, B. W. 1981. *Meso-scale atmospheric circulations*. Academic Press, London, 495 pp.

Billing, H. Haupt, I. and W. Tonn, 1983. Evolution of a hurricane-like cyclone in the Mediterranean Sea. *Beitr. Phys. Atmos.* **56**, 508–510.

Blier, W. and Q. Ma, 1996. Mediterranean sea tropical storms? *15th Conf. on Weather analysis and forecasting*, P5.9, 19–24 August, Norfolk, VA. Amer. Meteor. Soc., Boston, MA, USA.

Bosart, L. F. 1983. Analysis of California Catalina eddy event. *Mon. Wea. Rev.* **111**, 1619–1633.

Douglas, S. G. and R. C. Kessler, 1991. Analysis of mesoscale airflow patterns in the south-central coast air basin during the SCCCAMP 1985 intensive measurements periods. *J. Appl. Meteor.* **30**, 607–631.

Doyle, J. D. and T. T. Warner, 1993. Non-hydrostatic simulations of coastal meso-beta-scale vortices and frontogenesis. *Mon. Wea. Rev.* **121**, 3371–3392.

Ernst, J. A. and M. Matson, 1983. A Mediterranean tropical storm? *Weather* **38**, 332–337.

Grell, G. A., J. Dudhia and D. R. Stauffer, 1994. *A description of the fifth-generation Penn State/NCAR meso-scale model (MM5)*. NCAR Technical Note, NCAR/TN-398 + STR.

Kessler, R. C. and S. G. Douglas, 1991. A numerical simulation of meso-scale eddy development over the Santa Barbara Channel. *J. Appl. Meteor.* **30**, 633–651.

Mass, C. F. and M. D. Albright, 1989. Origin of the Catalina eddy. *Mon. Wea. Rev.* **117**, 2406–2436.

Mayengon, R. 1984. Warm core cyclones in the Mediterranean Sea. *Mar. Wea. Log.* **28**, 6–9.

Rasmussen, E. and C. Zick, 1987. A sub-synoptic vortex over the Mediterranean with some resemblance to polar lows. *Tellus* **39A**, 408–425.

Schär, C. and H. Wernli, 1993. Structure and evolution of an isolated semi-geostrophic cyclone. *Quart. J. Roy. Meteor. Soc.* **119**, 57–90.

Scorer, R. and A. Verkaik, 1989. *Spacious skies*. David & Charles Publishers, Newton Abbot Davon, Portugal, 192 pp.

Stein, U. and P. Alpert, 1991. Inclusion of sea moisture flux in the Anthes-Kuo cumulus parameterization. *Contri. Atmos. Phys.* **6**4, 231–243.

Stein, U. and P. Alpert, 1993. Factor separation in numerical simulations. *J. Atmos. Sci.* **50**, 2107–2115.